Evidence of spin-disorder scattering in liquid gold-iron alloys

1994 J. Phys.: Condens. Matter 6 603

(http://iopscience.iop.org/0953-8984/6/3/003)

J. Phys.: Condens. Matter 6 (1994) 603–612. Printed in the UK

Evidence of spin-disorder scattering in liquid gold–iron alloys

P Terzieff† and J G Gasser‡

† Institut für Anorganische Chemie, Universität Wien, Währingerstraße 42, A-1090 Wien, Austria

‡ Laboratoire de Physique des Liquides et des Interfaces, Université de Metz, 1 Boulevard Arago, 57070 Metz, France

Received 19 July 1993, in final form 5 October 1993

Abstract. The influence of small additions of iron on the electrical resistivity of liquid gold has been investigated for an iron content $x_{Fe} \leqslant 0.24$. The drastic increase in the resistivity due to small amounts of iron as well as the negative temperature coefficient apparent in the more concentrated alloys are not understandable on the basis of the Faber–Ziman formalism. The localization of large magnetic moments on the impurity atoms is assumed to be responsible for this exceptional behaviour. A tentative description is presented in terms of spin-disorder scattering including some particular aspects of the Kondo effect.

1. Introduction

It is generally accepted that the transport properties of liquid metals and alloys are, at least qualitatively, well explained by the Faber–Ziman theory, either in the original version [1] or the t-matrix formulation put forward by Evans *et al* [2]. Thus, many of the characteristic features of noble-metal-based systems, e.g. resistivity maxima at certain compositions or negative temperature coefficients in alloys with polyvalent metals, are attributed to the systematic variation in the Fermi vector k_F with respect to the position of the first maxima in the partial structure factors.

Even alloys with transition metals have been successfully treated by this formalism. On the assumption that the transition metals are monovalent, the electronic behaviour of liquid noble-metal–transition-metal alloys can be classified to be that of the Au–Ag group, i.e. because of an almost constant k_F the resistivities are expected to vary smoothly with the composition and the temperature coefficients are predicted to be positive throughout the phase diagram [3]. The distinctly different behaviour of the liquid Cu–Mn alloys—at high manganese concentrations ($x_{Mn} \geqslant 0.2$) the resistivity definitely decreases with increasing temperature—has been considered to be an exception. Magnetically, on the other hand, the manganese atoms are distinguished by very high, well localized magnetic moments associated with a spin number S of about $\frac{5}{2}$ [4]. It is obvious that the 'exceptional' behaviour of liquid Cu–Mn has to be assigned to the interactions between the localized spin and conduction electrons (s–d interactions).

Apparently, the usual classification scheme does not apply to those noble-metal–transition-metal systems where such strong localized magnetic moments are formed. Within this context, liquid Au–Fe should be another candidate for such 'exceptional' behaviour, since with $\frac{3}{2} < S < \frac{5}{2}$ its magnetic behaviour is comparable with that of Cu–Mn. In fact, the electrical resistivity was reported to increase dramatically on the addition of iron, and some alloys even exhibited an almost temperature-independent resistivity [3].

0953-8984/94/030603+10$07.50

In continuation of our previous study on the magnetic properties of liquid Au–Fe alloys [5], and in order to substantiate our arguments concerning the classification of this particular class of systems, we decided to reinvestigate carefully the electrical resistivity of the system with special emphasis on the sign of the presumably small temperature coefficient.

2. Experimental details

The electrical resistivities have been determined by a capillary method. All measurements were performed in suitably designed quartz cells under argon at a pressure of up to about 2 bar. The current supply and the recording of the voltage drop across the capillary were provided by four tungsten electrodes; the temperatures were controlled by a set of chromel–alumel thermocouples attached directly to the capillary. The calibration of the cells was performed at room temperature using high-purity mercury as the reference liquid ($\rho = 95.783\ \mu\Omega$ cm; $d\rho/dT = 0.89\ n\Omega$ cm K^{-1}).

Two series of measurements have been performed, using two different cells and always starting with pure liquid gold. The composition of the alloys was continually changed by dropping one of the pure components (gold slugs of purity 99.999% from Johnson Matthey; iron wire of purity 99.98% from Johnson Matthey) into the cell. In order to have better control of unwanted chemical side reactions (oxidation of the alloy, reaction with the electrodes, etc) the concentration of Fe was changed in a non-systematic manner; in the first cell the Fe content was progressively increased from $x_{Fe} = 0.03$ to 0.12 in steps of 0.03 while, in the other, x_{Fe} was varied in the sequence 0.12, 0.18, 0.24, 0.21, 0.18 and 0.15. Within our experimental accuracy of about 1%, the two sets of data yielded very consistent results.

3. Results and discussion

Because of the high melting point of Au on the one side, and the limited high-temperature stability of quartz on the other side, our measurements were confined to a relatively narrow temperature region of about 1300–1450 K. The most characteristic features of the system are apparent from figure 1 which gives a summarized representation of the results, and also from figures 2 and 3 which show the details as a function of Fe content at our reference temperature of 1400 K; the resistivities increase dramatically on the addition of Fe, and the temperature coefficients change sign at $x_{Fe} \simeq 0.08$. As regards the variation in the resistivity with the concentration, our findings are fully compatible with the earlier investigations of Günterhodt and Künzi [3] (figure 2) who suggested a maximum at $x_{Fe} \simeq 0.6$. In fact, our value obtained at $x_{Fe} = 0.24$ is already of the same magnitude as that of pure Fe extrapolated to our reference temperature [6]. Concerning the temperature dependence, their results imply negligible temperature coefficients for alloys with $x_{Fe} \geqslant 0.15$ whereas our own measurements, presumably owing to a better experimental resolution, yielded likewise small but clearly negative temperature coefficients for $x_{Fe} \geqslant 0.08$. Although it is not evident from figure 1, the relationship between the resistivity and the temperature is in general not strictly linear; therefore the experimental data have been fitted by polynomials up to the second order; the coefficients are listed in table 1.

This very characteristic shape of the resistivity versus Fe content curve and the appearance of negative temperature coefficients are typical and well explained features of noble-metal–polyvalent-metal alloys; however, it is striking to find such a distinctive behaviour in a noble-metal–transition-metal system.

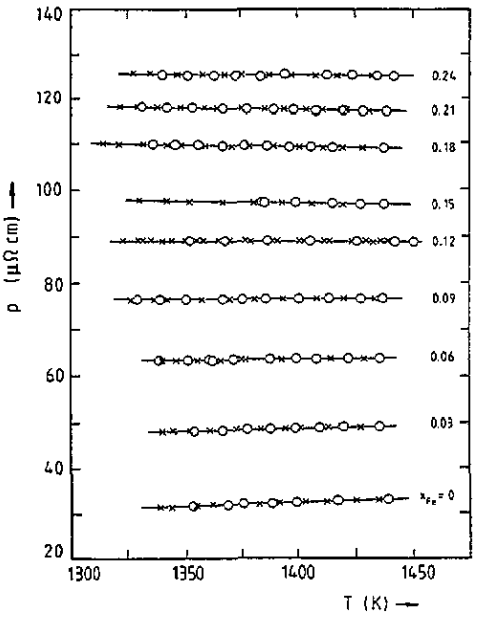

Figure 1. Electrical resistivity of liquid gold–iron alloys as a function of temperature and Fe content: ○, heating; ×, cooling.

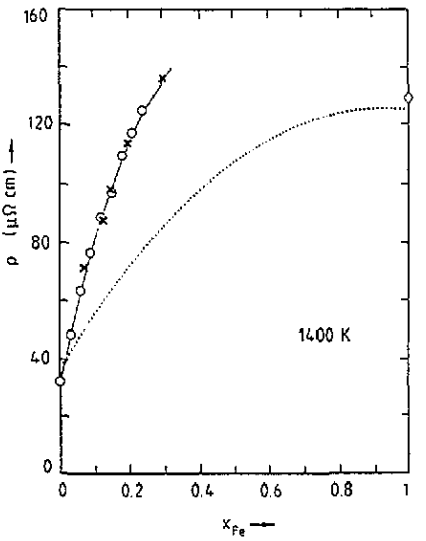

Figure 2. Electrical resistivity of liquid gold–iron alloys as a function of Fe content at 1400 K: ○, experimental values, this work; ×, data taken from [3] (1373 K); ◇, taken from [6], ·····, Faber–Ziman theory [1, 2].

3.1. Resonance scattering

In the past, the electrical resistivities of liquid alloys have been successfully derived from the Faber–Ziman [1] theory. If resonance scattering is the dominating process, the resistivity of a binary liquid alloy can be written as [2]

$$\rho_{\mathrm{res}} = \frac{3\pi m^{*2}\Omega}{4e^2\hbar^3 k_{\mathrm{F}}^2}\int_0^1 \mathrm{d}\left(\frac{q}{2k_{\mathrm{F}}}\right) 4\left(\frac{q}{2k_{\mathrm{F}}}\right)^3 |T_{\mathrm{all}}|^2 \tag{1}$$

The quantity $|T_{\mathrm{all}}|^2$ is determined by the partial structure factors a_{ij} and the **t**-matrices, according to

$$|T_{\mathrm{all}}|^2 = c_1\mathbf{t}_1^2[c_2 - c_1 a_{11}(q/2k_{\mathrm{F}})] + c_2\mathbf{t}_2^2[c_1 - c_2 a_{22}(q/2k_{\mathrm{F}})] + c_1 c_2(\mathbf{t}_1^*\mathbf{t}_2 + \mathbf{t}_1\mathbf{t}_2^*)[1 - a_{12}(q/2k_{\mathrm{F}})]. \tag{2}$$

The **t**-matrices of the constituents are related to the phase shifts $\eta_l(E_{\mathrm{F}})$ of the individual partial waves and the Legendre polynomials $P_l(\cos\theta)$ via

$$\mathbf{t}\left(E_{\mathrm{F}}, \frac{q}{2k_{\mathrm{F}}}\right) = -\frac{2\pi h^3}{m^*(2m^*E_{\mathrm{F}})^{1/2}}\frac{1}{\Omega}\sum(2l+1)\sin\eta_l \exp(\mathrm{i}\eta_l)\, P_l(\cos\theta). \tag{3}$$

In fact, if we apply this formalism to describe the resonance scattering resistivity in liquid Au–Fe alloys, we arrive at inadequate theoretical predictions. The calculated curves shown

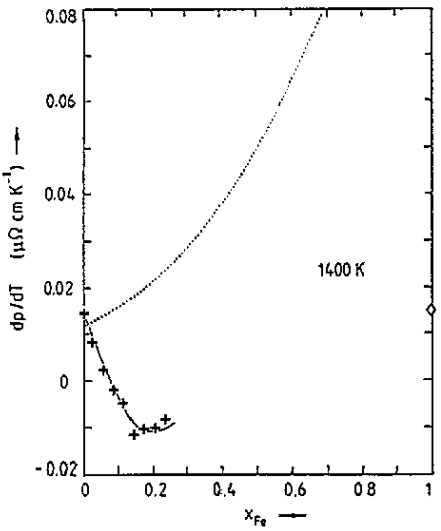

Figure 3. Temperature coefficient of the electrical resistivity in liquid gold–iron alloys as a function of Fe content at 1400 K: +, experimental values, this work; ◊, experimental value taken from [6]; ·····, Faber–Ziman theory [1, 2].

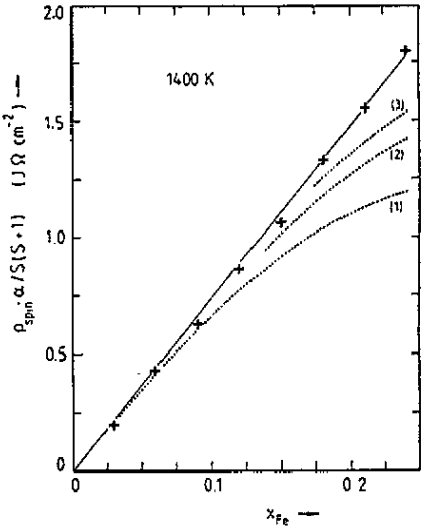

Figure 4. The combined quantity $\rho_{spin}a/S(S+1)$ in liquid gold–iron alloys as a function of Fe content at 1400 K: +, obtained directly from the experimental values ($\rho_{spin} = \Delta\rho$); ·····, deduced with the inclusion of resonance scattering ($\rho_{spin} = \Delta\rho - \Delta\rho_{res}$) calculated for different band widths Γ (curve (1), 0.8 eV; curve (2), 1.6 eV; curve (3), 2.0 eV).

Table 1. Coefficients of the least-squares fit to the electrical resistivities of liquid gold–iron alloys: ρ ($\mu\Omega$ cm) $= a_0 + a_1T + a_2T^2$ (T in K).

x_{Fe}	a_0	$a_1 \times 10^3$	$a_2 \times 10^6$
0	11.98	14.66	—
0.03	36.77	8.52	—
0.06	59.78	2.62	—
0.09	78.58	−1.54	—
0.12	116.35	−33.28	10.42
0.15	180.91	−102.60	32.98
0.17	174.91	−79.54	25.27
0.21	159.55	−48.02	13.81
0.24	177.74	−63.41	20.01

in figures 2 and 3 were obtained by assuming the phase shifts to be independent of the composition and the structure to be well described by the hard-sphere structure factors of Ashcroft and Langreth [7]. The phase shifts ($\eta_0 = -0.425$, $\eta_1 = -0.093$ and $\eta_2 = 2.983$ for Au; $\eta_0 = -0.392$, $\eta_1 = -0.029$ and $\eta_2 = 2.748$ for Fe), the packing fractions (0.4524 for Au; 0.5170 for Fe), the effective-mass ratio m^*/m (0.71 for Au; 0.80 for Fe), as well as the procedure for evaluating E_F were those proposed by Waseda [8]; the atomic volumes Ω of the components (18.975×10^{-30} m^3 for Au; 12.564×10^{-30} m^3 for Fe) were taken from the compilation of Crawley [9]. For alloys, the volume, the effective mass and the Fermi energy were considered to vary linearly with composition.

The discrepances are evident; the actual increase in resistivity due to the addition of Fe is much larger than predicted, and the trend in the temperature coefficient is even opposite

to that derived from theory. To a large degree, the divergences apparent on the Fe-rich side of figure 3 are due to the extrapolation of the input data from above 1800 K down to our reference temperature of 1400 K. It is difficult to estimate to what extent the shortcoming of the theory is due to the severe simplifications in evaluating equations (1)–(3).

There are strong indications that the d-wave phase shift η_2 of Fe in dilute alloys, one of the essential ingredients of the theory, is different from that in concentrated alloys. Previous magnetic measurements have shown that the filling of the d bands in dilute liquid Au–Fe alloys, and therefore the d-wave phase shift, varies with composition and is definitely different from that of pure liquid Fe [5]. In fact, the d-wave phase shift quoted by Waseda [8] is absolutely incompatible with the pronounced magnetic behaviour of Fe in liquid Au. The exceptionally high spin S of about $\frac{5}{2}$ per Fe atom points clearly towards a large splitting of the impurity levels into a nearly filled spin-up level ($Z_\uparrow \simeq 5$) and a nearly empty spin-down level ($Z_\downarrow \simeq 0$). As a consequence, since $\eta_{\uparrow,\downarrow} = \frac{1}{5}\pi Z_{\uparrow,\downarrow}$, the phase shifts $\eta_\uparrow \simeq \pi$ and $\eta_\downarrow \simeq 0$ give a contribution on the electrical resistivity even smaller than that obtained with the phase shifts recommended by Waseda [8].

Although we may assume that resonance scattering still gives an important contribution and that the Faber–Ziman theory, if applied in a more correct form, might give appropriate results, we shall try to understand our experimental results in terms of spin-disorder scattering, i.e. those effects due to interactions between the spins of the localized d electrons and the conduction electrons.

For our further argumentation we shall treat the experimentally determined residual resistivity $\Delta\rho(= \rho - \rho^{\mathrm{Au}})$ as a superposition of a resonance scattering term $\Delta\rho_{\mathrm{res}}(= \rho_{\mathrm{res}} - \rho_{\mathrm{res}}^{\mathrm{Au}})$ and a spin-disorder scattering term ρ_{spin} according to

$$\Delta\rho = \Delta\rho_{\mathrm{res}} + \rho_{\mathrm{spin}}. \tag{4}$$

3.2. Spin-disorder scattering

If resonance scattering is completely neglected ($\Delta\rho_{\mathrm{res}} \simeq 0$; $\Delta\rho \simeq \rho_{\mathrm{spin}}$), the residual resistivity should be directly related to $S(S+1)$ and the s–d interaction energy J_{eff} [10]:

$$\rho_{\mathrm{spin}} = \tfrac{3}{2}\pi(m^*/he^2)(\Omega/E_{\mathrm{F}})x_{\mathrm{Fe}}S(S+1)J_{\mathrm{eff}}^2. \tag{5}$$

It is evident from figure 4 that the combined quantity $\rho_{\mathrm{spin}}a/S(S+1)$ varies linearly with the Fe content x_{Fe} ($a = mE_{\mathrm{F}}/m^*\Omega$). This is indeed the behaviour predicted by equation (5), indicating that J_{eff} is about the same for all compositions. From the slope we deduce an s–d interaction energy of $|J_{\mathrm{eff}}| = 1.33$ eV which corresponds roughly to the average value of about 1.5 eV deduced for concentrated and dilute solid transition-metal alloys [11]. Our value is of the correct order of magnitude but, since resonance scattering has been ignored, it represents rather the upper limit of J_{eff}.

3.3. Resonance scattering and spin-disorder scattering

In order to determine the s–d interaction energy J_{eff} more precisely, we may include a finite resonance scattering contribution. A fully theoretical calculation of the actual phase shifts in our alloys goes beyond the scope of this paper; however, we may derive some estimates in a semi-empirical manner from the Friedel–Anderson [12] model. In this concept, the magnetically split impurity states are considered to have a Lorentzian shape of an effective

width Γ being centred at $E_\uparrow - E_F$ and $E_\downarrow - E_F$, respectively. The d-wave phase shifts $\eta_\uparrow$ and $\eta_\downarrow$ are related to these basic quantities via

$$\eta_\uparrow = \tan^{-1}[\Gamma/2(E_\uparrow - E_F)] \qquad \eta_\downarrow = \tan^{-1}[\Gamma/2(E_\downarrow - E_f)]. \tag{6}$$

Strictly, the problem is to find good estimates for Γ, $E_\uparrow - E_F$ and $E_\downarrow - E_F$. Following the theory, the difference in the phase shifts as well as the splitting of the impurity levels can be expressed in terms of the spin S according to

$$\eta_\uparrow - \eta_\downarrow = \tfrac{2}{5}\pi S \qquad E_\uparrow - E_\downarrow = \tfrac{1}{5} S U_{\text{eff}}. \tag{7}$$

For the exchange energy we assumed that $U_{\text{eff}} \simeq 7$ eV which is about the average of the values quoted in the literature (6.5–7 eV [13] and 7–7.5 eV [14]). Thus, by combining equations (6) and (7) with the experimental values of S and assigning a fixed value to Γ, a complete set of model parameters can be established, in consistency with the magnetic properties of the system. The choice of $\Gamma = 0.8$ eV takes account of the widths actually observed in solid dilute **Au**Cr (0.7 eV), **Au**Ni (0.6 eV) or **Ag**Mn (0.8 eV) [15]. In order to take account of impurity levels broader than those in solid alloys, additional calculations with $\Gamma = 1.6$ and 2.0 eV were performed in the same manner. Table 2 lists a typical set of parameters obtained for $\Gamma = 0.8$ eV.

Table 2. Spin S, positions $E_\uparrow - E_F$ and $E_\downarrow - E_F$ of the magnetically split d states, and the d-wave phase shifts $\eta_\uparrow$ and $\eta_\downarrow$ of liquid gold–iron alloys deduced from equations (6) and (7) for a full width of $\Gamma = 0.8$ eV.

x_{Fe}	S	$E_\uparrow - E_F$ (eV)	$E_\downarrow - E_F$ (eV)	$\eta_\uparrow$	$\eta_\downarrow$
0.03	2.261	−1.862	4.469	2.930	0.089
0.06	2.108	−0.914	4.988	2.729	0.080
0.09	2.094	−0.869	4.994	2.710	0.080
0.12	2.010	−0.677	4.951	2.608	0.082
0.15	1.947	−0.569	4.882	2.529	0.082
0.18	1.903	−0.507	4.821	2.474	0.083
0.21	1.854	−0.449	4.742	2.414	0.084
0.24	1.80*	−0.393	4.647	2.348	0.086

* Extrapolated.

Because of the arbitrariness in selecting the values of Γ the results are not unique, but, irrespective of the choice of Γ, the positions of the majority levels $E_\uparrow - E_F$ coincide roughly with those of solid **Au**Cr (−0.91 eV), **Au**Ni (−0.4 eV) and **Ag**Mn (−2.8 eV) [15]. The systematic variation with composition is primarily a consequence of assuming a constant width for all concentrations.

It is not clear whether equations (1)–(3) also apply to a magnetically split structure; however, as a first attempt we modified the procedure by splitting all terms in equation (3) containing η_2 into an $\eta_\uparrow$ and an $\eta_\downarrow$ part. The results for ρ_{res} obtained with $\Gamma = 0.8$ eV are compiled in table 3, together with the experimental resistivities ρ, the spin scattering resistivity ρ_{spin} deduced from equation (4), the quantity a, and the interaction energy J_{eff} evaluated with the help of equation (5).

Figure 5 gives a summarized graphical representation of the residual resistivities obtained with the different choices of Γ, compared with the experimental values. It is

Table 3. Electrical resistivities of liquid gold–iron alloys and some deduced quantities at 1400 K: the experimental restivities ρ, the resonance scattering resistivities ρ_{res} calculated for a d-level width of $\Gamma = 0.8$ eV, the deduced spin scattering contributions ρ_{spin}, the quantity $a = mE_F/m^*\Omega$, and the s–d interaction energies J_{eff}.

x_{Fe}	ρ	ρ_{res} ($\mu\Omega$ cm)	ρ_{spin} ($\mu\Omega$ cm)	a (10^{10} J m^{-3})	J_{eff} (eV)
0	32.46	37.68	0	9.03	—
0.03	48.70	37.48	16.44	9.12	−1.29
0.06	63.45	37.81	30.86	9.21	−1.33
0.09	76.43	39.56	42.09	9.30	−1.28
0.12	88.64	43.02	50.84	9.40	−1.27
0.15	97.01	48.09	54.14	9.50	−1.21
0.18	109.34	54.40	60.16	9.60	−1.19
0.21	117.34	61.46	61.10	9.71	−1.15
0.24	125.23	68.73	61.72	9.82	−1.11

evident that, at small concentrations, resonance scattering is negligible, which justifies the assumption $\Delta\rho_{res} \simeq 0$ made in the preceding section. At higher concentrations, $\Delta\rho_{res}$ increases rapidly at the expense of ρ_{spin}, at a rate dependent on the choice of Γ. As a result, $|J_{eff}|$ remains constant (about 1.3 eV) up to a certain limit ($x_{Fe} \simeq 0.12$ for $\Gamma = 0.8$ eV) and decreases with further increase in x_{Fe} to about 1.1 eV at $x_{Fe} = 0.24$ (table 3). This is also reflected by the decreased slope of the $\rho_{spin}a/S(S+1)$ versus x_{Fe} curve at higher Fe contents (figure 4).

3.4. Temperature coefficient

Concerning the unexpected temperature dependence of the electrical resistivity, we may find an explanation in terms of the Faber–Ziman theory if a higher valence of the transition metal is taken into consideration. In such a case, Au–Fe would behave typically like any other noble-metal–polyvalent-metal system. Chemically, and in view of the high spin $S \simeq 1.8$–2.3, it would indeed be plausible to consider Fe in the divalent or even trivalent state; however, in our understanding this is not a very realistic picture.

Although the negative temperature coefficients do not fit the usual classification scheme, the behaviour of Au–Fe is not unique; in fact, there is a very strong similarity to the system Cu–Mn, in both the liquid and the solid state. The negative temperature coefficients of the resistivity, the similar high spin numbers [4, 5], as well as the Kondo-like behaviour in the solid state [10] or the very pronounced tendency to form spin glasses [16] are features common to both systems. It is doubtful whether the concept of the Kondo effect can be applied to rather concentrated liquid alloys but, since we have no better interpretation, it was tempting to identify the unusual temperature dependence as a Kondo-like behaviour. In the high-temperature limit the spin-disorder resistivity would then be expected to vary logarithmically with temperature [10]:

$$\mathrm{d}\rho_{spin}/\mathrm{d}\log T) = 3z\rho_{spin}J_{eff}/E_F. \tag{8}$$

z denotes the number of valence electrons per atom; in our special case we assumed that $z \simeq 1$. To be more correct, this term should have been included in equation (5), but its absolute contribution is only very small and has almost no influence on our further reasoning. It is indeed a remarkable experimental observation that, at all compositions, the residual resistivity $\Delta\rho$ decreases with increasing temperature, in more concentrated alloys in a non-linear and presumably even logarithmic manner.

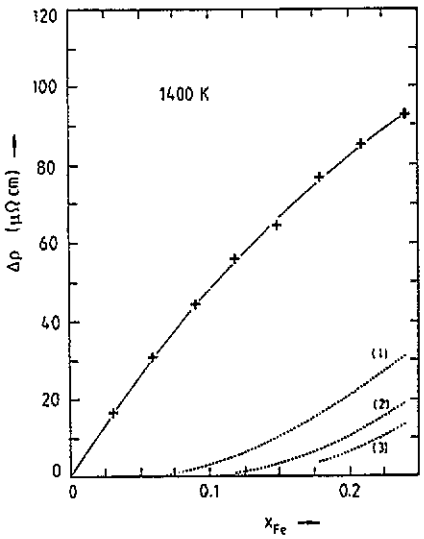

Figure 5. Residual resistivity $\Delta\rho$ of liquid gold–iron alloys at 1400 K: +, experimental values; ·····, calculated in the resonance scattering approach for different band widths Γ (curve (1), 0.8 eV; curve (2), 1.6 eV; curve (3), 2.0 eV).

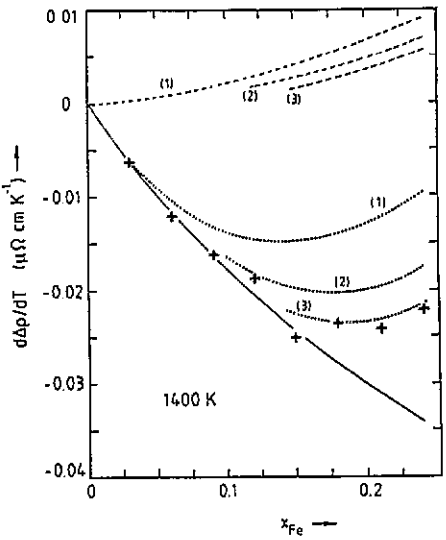

Figure 6. Temperature coefficient of the residual resistivity in liquid gold–iron alloys as a function of Fe content at 1400 K: +, experimental values; ——, spin-disorder contribution deduced for $\Delta\rho_{res} = 0$; - - - -, contribution from resonance scattering; ·····, superposition of resonance and spin scattering contribution for different band widths Γ (curve (1), 0.8 eV; curve (2), 1.6 eV; curve (3), 2.0 eV).

So far, the sign of J_{eff} has not been discussed; however, the negative temperature coefficient of $\Delta\rho$ (figure 6) points towards a negative value of J_{eff} which extending from -1.1 to -1.3 eV (table 3) is now of about the same magnitude as those deduced for solid **Cu**Cr (-1.2 eV [17]), solid **Au**V (-0.6 eV [18]) or solid **Au**Co (-0.63 eV [19]), but higher than in solid **Au**Fe (-0.25 eV) or solid **Cu**Fe (-0.4 eV) [20]. If we now evaluate equation (8) at our reference temperature of 1400 K, we arrive at surprisingly good agreement with the experiment; the most relevant numerical values are listed in table 4. The temperature coefficients shown in figure 6 refer to residual quantities, i.e. $d(\Delta\rho)/dT$ as obtained from the experiment, $d(\Delta\rho_{res})/dT$ originating from resonance scattering, and the sum of $d(\Delta\rho_{res})/dT$ and $d\rho_{spin}/dT$ evaluated for the different values of Γ. The experimental curve is already well reproduced if the residual resistivity is completely assigned to spin-disorder scattering ($\Delta\rho_{res} = 0$; $J_{eff} = -1.33$ eV). The inclusion of a resonance scattering contribution ($\Gamma = 0.8$, 1.6 or 2.0 eV) even reproduces the convex portion of the experimental curve.

The best agreement is apparently achieved with $\Gamma = 2$ eV; however, with such a choice of Γ, equations (6) and (7) cannot be solved for small concentrations of Fe, at least not for the boundary conditions imposed by the spin S. It is obvious that the most acceptable fit to the experimental data can be obtained, if Γ is assumed to increase with increasing x_{Fe}. This is indeed a reasonable assumption, since Γ is expected to increase with increasing electronic density of states; however, we abstained from exaggerating our rather crude picture in too much detail.

Table 4. Temperature coefficients of the electrical resistivities in liquid gold–iron alloys at 1400 K: the experimental values $d\rho/dT$, the resonance scattering contributions $d\rho_{res}/dT$ calculated for $\Gamma = 0.8$ eV and the spin scattering contributions $d\rho_{spin}/dT$ deduced from equation (8).

x_{Fe}	$d\rho/dT$ (10^{-10} Ω m K^{-1})	$d\rho_{res}/dT$ (10^{-10} Ω m K^{-1})	$d\rho_{spin}/dT$ (10^{-10} Ω m K^{-1})	
			Without $\Delta\rho_{res}$[a]	With $\Delta\rho_{res}$[b]
0	1.47	1.18	—	—
0.03	0.85	1.23	−0.61	−0.60
0.06	0.26	1.28	−1.16	−1.15
0.09	−0.15	1.36	−1.64	−1.51
0.12	−0.41	1.47	−2.08	−1.80
0.15	−1.03	1.60	−2.38	−1.82
0.18	−0.88	1.74	−2.83	−1.98
0.21	−0.94	1.91	−3.11	−1.93
0.24	−0.74	2.10	−3.39	−1.88

[a] Calculated with $\Delta\rho_{res} = 0$ ($J_{eff} = -1.33$ eV).
[b] Calculated with the inclusion of $\Delta\rho_{res}$ ($\Gamma = 0.8$ eV; J_{eff} from table 3).

4. Conclusion

The Faber–Ziman formalism, either in its original form or in the resonance scattering approach, yields only an incomplete description of magnetic transition-metal alloys such as Au–Fe or Cu–Mn. In these particular cases the more or less drastic increase in the resistivity on the addition of the transition metal as well as the negative temperature coefficient seem to be associated with the appearance of strongly localized spins. As a consequence, the usual classification scheme based on the formal valences of the components seems to be inadequate for this particular class of alloys. There are strong indications that, in such magnetically distinguished systems, s–d interactions play the dominant role.

In order to substantiate the arguments put forward in this paper, it would be of special interest to have this category of liquid alloys reinvestigated in a more systematic manner by different experimental techniques. From a theoretical point of view, it is not very clear whether the concept of spin-disorder scattering really applies to liquid transition-metal alloys. Furthermore, it would be profitable to know whether for principal reasons or for inappropriate input parameters the Faber–Ziman theory fails to explain the behaviour of this class of liquid alloys.

Acknowledgments

The authors want to thank Professor N E Cusack and Professor H J Güntherodt for their interest in this paper and their encouraging comments.

References

[1] Faber T E and Ziman J M 1965 *Phil. Mag.* **11** 153
[2] Evans R, Greenwood D A and Lloyd P 1971 *Phys. Lett.* **35A** 57
Dreirach O, Evans R, Güntherodt H J and Künzi H U 1972 *J. Phys. F: Met. Phys.* **2** 709
[3] Güntherodt H J and Künzi H U 1973 *Phys. Kondens. Mater.* **16** 117
[4] Nagakawa Y 1959 *J. Phys. Soc. Japan* **14** 1372

[5] Terzieff P and Wachtel E 1991 *J. Mater. Sci.* **27** 3359
[6] Kita Y, Ohguchi S and Morita Z 1978 *J. Iron Steel Inst. (Japan)* **64** 711
[7] Ashcroft N W and Langreth D C 1967 *Phys. Rev.* **159** 500
[8] Waseda Y 1980 *The Structure of Non-Crystalline Materials* (New York: McGraw-Hill)
[9] Crawley A F 1974 *Int. Metall. Rev.* **19** 32
[10] Kondo J 1964 *Prog. Theor. Phys.* **32** 37
[11] Weiss R J and Marotta A S 1959 *J. Phys. Chem. Solids* **9** 302
[12] Friedel J 1956 *Can. J. Phys.* **34** 1190
Anderson P W 1961 *Phys. Rev.* **124** 41
[13] Yoshida K, Okiji A and Chikazumi S 1965 *Prog. Theor. Phys.* **33** 559
[14] Klein A P and Heeger A J 1966 *Phys. Rev.* **144** 458
[15] Reehal H S and Andrews P T 1980 *J. Phys. F: Met. Phys.* **10** 1631
[16] Beck P A 1978 *Prog. Mater. Sci.* **23** 1
[17] Coleridge P T, Scott G B and Templeton I M 1972 *Can. J. Phys.* **50** 1999
[18] Kume K 1967 *J. Phys. Soc. Japan* **23** 1225
[19] Loram J W, Ford P J and Whall T E 1970 *J. Phys. Chem. Solids* **31** 763
[20] Loram J W, Whall T E and Ford P J 1970 *Phys. Rev.* B **2** 857